ACS APPLIED MATERIALS & INTERFACES

Research Article

www.acsami.org

High-Performance Nanothermite Composites Based on Aloe-Vera-Directed CuO Nanorods

Vinay Kumar Patel and Shantanu Bhattacharya*

Microsystems Fabrication Laboratory, Department of Mechanical Engineering, Indian Institute of Technology Kanpur, Kanpur 208016, Uttar Pradesh, India

Supporting Information

ABSTRACT: In this work, we demonstrate the development of high-performance nanothermite composites derived from super-reactive CuO nanorods oxidizers fabricated by simple biogenic routes using Aloe vera plant extracts. Nanorods of various length scales have been realized via simple sonoemulsion and solid-state biosynthesis routes using Aloe vera gel as a green surfactant promoting the directional growth of CuO nanorods in both solid and emulsion phase. The biosynthesized CuO nanorods (oxidizers)/fuel (nanoaluminum) composites ignited vigorously with abundant gas generation, developing high heat of reaction of 1.66 kJ g^{-1} and very high pressurization rate of around 1.09 MPa μs^{-1} and peak pressure of 65.4 MPa when blasted inside a constant volume pressure cell with a charge density of 0.2 g cm^{-3}. The pressurization rates so obtained are four times higher with twice the peak pressure in comparison to such nanothermites formulated via other available state of the art wet-chemical techniques, which reflects the catalytic role of Aloe vera surface functional groups (A. vera-sfg) enhancing the reactivity of CuO oxidizers with excess gas release rate during exothermic reaction with nanoaluminum. Through this work, Aloe vera gel has for the first time been identified as a novel biotemplate for green synthesis of nanorod structures of metal oxides, and we have also studied the utility of A. vera-sfg in the creation of super-reactive CuO oxidizers producing excellent heat of reaction and dynamic pressure characteristics as demanded in propellants, explosives, and pyrotechnics.

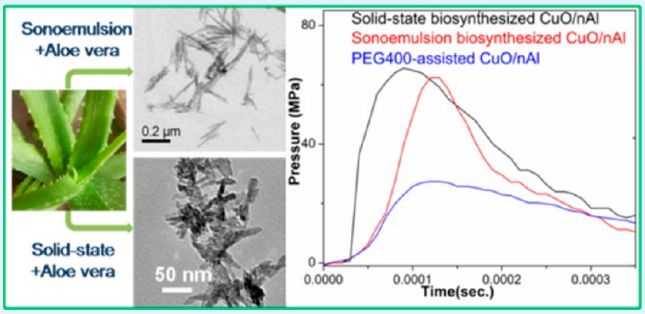

KEYWORDS: *copper oxide, nanorods, Al/CuO, nanothermite, nanoenergetic materials, combustion, heat of reaction*

1. INTRODUCTION

There has been a worldwide increase in societal interests toward nanotechnology with advancement in functional nanomaterials which are widely used in consumer and medical products. For synthesis of such materials, wet chemical methods have been widely explored utilizing stabilizing and/or reducing agents in liquid medium where an assembler of the products generated (also known as surfactant) is used to obtain directional synthesis of such material. Many of the assemblers, or surfactants as they are more commonly known, that are used for sustenance of directional growth of nanomaterials are toxic in nature or otherwise some industrial processes that are used in their manufacture involve highly carcinogenic and toxic chemicals or reagents for polymerization. The increasing usage of nanomaterials is very commonplace in the current business environment, and increased usage of these organic, polymeric, or inorganic surfactants impose serious threats to the ecosystems and environment. Hence, for sustainable development of nanotechnology, ecofriendly approaches and green biological methods should be rapidly explored.[1,2] Several research groups have successfully demonstrated the nanoscale synthesis of Ag, Au, and Pd nanoparticles from various plant leaf extracts, for example, neem,[3,4] lemon grass,[5] geranium leaves,[6] Krishna Tulsi,[7] Vinca rosea,[8] hibiscus cannabinus,[9] and so forth; plant fruit extract, for example, pear fruit extract,[10] Prunus domestica fruit extract,[11] solanum lycopersicums extract;[12] bark extract[13] and buds.[14] In recent years, a growing interest in biogenic synthesis of metal oxide nanoparticles has evolved by using biological entities such as bacteria, algae, fungi, and so forth as detailed by Duran and Seabra.[15] Medicinal plant extracts such as Aloe vera have been recently explored in the synthesis of metal oxides such as CuO,[16] ZnO,[17,18] In_2O_3,[19] Fe_xO_y,[20−22] and tin oxide[23] nanoparticles.

Among the various metal oxides, CuO (p-type semiconductor with band gap of 1.2 eV) is of great interest owing to its wide applications in heterogeneous catalysis,[24] gas sensing,[25] lithium electrode material,[26] solar cells,[27] reactive oxidizers in nanothermite composites,[28,29] and so forth. CuO has also been recognized as attractive oxygen carrier for capturing and separation of CO_2 with little energy loss in chemical looping combustion of fossil fuels and waste to reduce the greenhouse gas emissions.[30,31] So far, CuO nanorods have

Received: October 1, 2013
Accepted: November 27, 2013
Published: November 27, 2013

been prepared by various methods including solid-state reaction methods,[32] sonoemulsion methods,[33] hydrothermal methods,[34] electrochemical methods,[35] and thermal oxidation of copper in air,[36] yet simple and cost-effective solutions utilizing nontoxic ecofriendly biological precursors are not fully evolved.

Despite the wide popularity and historical reputation of the Aloe vera (Aloe barbadensis Miller) plant for its therapeutic effects, its extract has been less exploited in the synthesis of nanomaterials e.g. Au nanotriangles and Ag nanoparticles,[3] and CuO,[16] ZnO,[17] Fe_3O_4,[22] In_2O_3[19] nanoparticles etc. For a long time, the fresh Aloe vera gel, its juice and commercial products are utilized for health, medical and cosmetic applications.[37] Aloe vera gel constitutes the nutritive compounds of water/moisture (98.5−99.5%), soluble polysaccharides and free monosaccharides (0.25%), N2 protein, amino acids, glycoproteins (lectins with hemoagglutination activity), enzymes (aloctin A, aloctin B, bradykinase, carboxypeptidase, catalase, SOD, GSH-Px, peroxidase), vitamins (ascorbic acid, complex B: thiamin, riboflavin, niacin, folic acid carotenoids, tocopherols), minerals and electrolytes (K, Cl (Na), Ca, Mg, P), and trace elements (Fe, Cu, Zn, Mn, Al, Se, Cr).[38] In medical applications, Aloe vera is used as antipyretic,[39] antioxidative,[40] and cathartic.[41]

In this research Article, we have addressed for the first time the directional synthesis aspect of metal oxides utilizing the Aloe vera leaf gel. We have been able to produce high yield and high quality CuO nanorods via biogenic route using Aloe vera gel. We have also further characterized the increased thermal and combustion properties of these reactive oxides combined with aluminum nanoparticles. Although the basic materials that are being self-assembled are themselves biologically unfriendly but the approach of directional self-assembly using a naturally available extract eliminates the need of some very toxic precursors which were otherwise indispensable for obtaining directional self-assembly of nanomaterials.

Nanoassembled thermite composites are metastable intermolecular composites comprising a nanoscale metallic fuel and oxidizer (CuO, Fe_2O_3, Bi_2O_3, MoO_3, etc). These materials, when ignited, produce rapid release of heat and pressure by self-propagating combustion reaction throughout the whole material.[28,42] There are a wide range of combinations of metals and oxidizers for the formulation of such composites.[43] The aluminum nanopowder is widely used as a fuel element in these composites due to its low cost, availability, ease of manufacturing and favorable physical properties such as high reaction enthalpy, low vapor pressure, low melting temperature and high thermal conductivity etc.[44,45] The nanoscale self-assembly of such materials increases the surface contact between atomic clusters. Such high interfacial area leads to a decreased diffusion distance, reduced atomic length scale for heat and mass transfer, and so forth, leading to high ignition sensitivity and fast reaction/propagation rate with minimum heat loss.[46] The high speed of combustion coupled with high pressure/shock waves have found several defense and civilian applications like microthrusters,[47] safe arm and fire devices,[48] MEMS-based molecular delivery actuators,[49] and so forth. The energy density and combustion kinetics of nanothermite materials get significantly altered by a suitable combination of fuel and oxidizer of proper stoichiometry and right shape/size distribution. CuO nanorods have been widely explored as oxidizers in nanothermites owing to their low cost and simple fabrication methods and high theoretical heat of reaction resulting in high propagation rate of combustion.[28,50] In most of the CuO nanorod based nanothermite composites, the CuO nanorods have been developed by wet-chemical process using poly(ethylene glycol) of molecular weight 400 (PEG400) surfactant,[28,50,51] in which the self-propagating reaction rate has been found similar to that of some of the primary explosives. However, the low pressure generation associated with CuO nanorods/Al nanothermites required hybridization with ammonium nitrate and RDX[51] which are explosive materials, and as such their handling and control is hazardous and needs great precision and accuracy. In this Article, we have studied the combustion propagation rates and pressure−time characteristics of nanothermites consisting of aluminum nanopowder, and CuO nanorods synthesized by sonoemulsion and solid-state biosynthesis routes, and compared the combustion performance with standard synthesis techniques using PEG400 surfactant. We have observed a significant improvement in both peak pressure and pressurization rate which definitely makes the biosynthesized composites an ecofriendly alternative to standard synthesis techniques.

2. EXPERIMENTAL SECTION

Warning: Extreme precautions and proper safety protocols must be practiced during processing and testing of the nanothermites.

2.1. Materials. All chemicals used in the biogenic synthesis of CuO nanorods were analytical grade and used without any separate purification steps. Aluminum nanoparticles (average particle size, 80 nm) were procured from Neo Ecosystems and Software Private Ltd. India. The Aloe vera extract was collected directly from the inner gel portion of the Aloe vera leaves. The outer hard green layer of Aloe vera leaves was stripped (sliced) off to get the inner portion of the Aloe vera gel. The inner portion of the gel was finely crushed and ground into thin jelly form which was further filtered with a fine mesh cotton cloth.

2.2. Sonoemulsion Biosynthesis of CuO Nanorods. Sonoemulsion biosynthesis was a process similar to the standard sonoemulsion method[33] wherein a nonionic surfactant like poly(ethylene glycol) of molecular weight 8000 (PEG8000) has been replaced by Aloe vera gel. In this process, two precursor emulsion solutions were prepared by adding Aloe vera gel. The first emulsion was prepared by dissolving $CuCl_2{\cdot}2H_2O$ (1.705 g) in deionized water (10 mL). This was thoroughly mixed with Aloe vera gel (1.5 mL) with continuous stirring (using a magnetic bead and hot plate set to room temperature) for a minimum duration of 0.5 h. Similarly, a second emulsion solution of precursor KOH of quantity (1.68 g) was prepared and poured drop-by-drop in the first emulsion placed in a high frequency (42 kHz) ultrasonic bath set at 60 °C. After completion of pouring, an excess amount of 2-propanol (about 100 mL) was added immediately into the solution and was further ultrasonicated for about 30−45 min. The as-obtained black color precipitate was filtered and washed several times with deionized water and ethanol to remove the impurity of salts and Aloe vera. Finally, it was dried at 90 °C in an oven for 6 h to collect a residue of black dry powder of CuO.

2.3. Solid-State Biosynthesis of CuO Nanorods. In this method, CuO nanorods were synthesized by solid-state mixing of $CuCl_2{\cdot}2H_2O$ and NaOH in the presence of aloe vera gel. The synthesis involved the mechano-chemical mixing of $CuCl_2{\cdot}2H_2O$ (3.41 g) with NaOH (2 g) in the presence of Aloe vera gel (3 mL) using a mortar and pestle. Mixing was carried on until a completely black colored slurry was observed (within 5 min duration). This slurry was washed thoroughly several times with deionized water and ethyl alcohol to remove the NaCl, Aloe vera, and any unreacted precursor. The as-cleaned precipitate was collected in a similar manner by filtering and drying for 6 h in a convection oven at 90 °C.

2.4. Solid-State Reaction Synthesis of CuO Nanorods. In solid-state reaction, the synthesis of CuO nanorods was prepared by following the one-sep reaction process using the ionic surfactant

PEG400 developed by Wang et al.[32] In the synthesis process, $CuCl_2 \cdot 2H_2O$ (5 g) and NaOH (3 g) were continuously stirred together in the presence of PEG400 (5 mL) in a mortar/pestle for about 0.5 h until a black slurry was observed. This slurry was washed several times with deionized water and ethanol to remove undesired byproducts of salts and unreacted precursor impurity. Finally, the precipitate was dried at 90 °C for 6 h in a convection oven to get the pure CuO nanorods.

2.5. Preparation of Nanothermites. Nanothermites of desired quantity were prepared by homogeneous mixing of accurately weighted CuO nanorods oxidizer with aluminum nanopowder in 2-propanol (30 mL) solution via ultrasonic wave-assisted sonication in a Sonics Vibra-Cell ultrasonic-processor (model VCX130, 130 W, 20 kHz, Sonics & Materials, Inc.) at different equivalence ratios.[52] The aluminum nanopowders in formulated nanothermites were of spherical shape with average diameter of 80 nm. The ultrasonication process promoted better homogeneous mixing of fuel and oxidizer by effectively dispersing through breaking apart the agglomerates. After ultrasonication for about 5−10 min by maintaining the on−off pulse equal to 10 s in order to avoid any thermal gradient within the solution, the well homogenized slurry was poured in a glass Petri dish and finally dried at 90 °C to evaporate the 2-propanol completely. The dried nanothermite composites were carefully scraped off and stored in vacuum before testing.

2.6. Material Characterization. The crystal structure and composition of CuO nanorods were determined by powder X-ray diffraction (XRD) analysis using PANalytical X'Pert Pro diffractometer in the 2θ range of 20−80 ° at scan rate of 0.02 s^{-1} with Cu Kα radiation (wavelength 1.5418 Å). The surface morphology of CuO nanorods was characterized by transmission electron microscopy (TEM) at an accelerating voltage of 200 kV using a FEI Technai, 20 UT instrument. The surface morphology of aluminum nanoparticles and its nanothermite composites with CuO nanorods were characterized by TEM.

The thermogravimetric mass change and heat of reaction of CuO nanoflakes/Al nanothermite composites were thermally characterized by thermogravimetry and differential scanning calorimetry (TG-DSC) study conducted on a Netzsch STA 449F3 instrument. The TG-DSC analysis was carried from room temperature to 800 °C at a heating rate of 10 °C min^{-1} under nitrogen gas flow (99.999% purity). A sample mass (less than 10 mg) of nanothermite composites was utilized for TG-DSC analysis.

The combustion wave speed measurement was carried out in a constant volume (0.8 cm^3) polycarbonate burn tube (inside diameter of 3.18 mm) experiment (Figure 1a). The burn tube was filled with 0.225 g of nanothermite composites and inserted in a rectangular steel/acrylic block (50 mm × 50 mm × 100 mm). The spark was initiated from one side of the tube via nichrome wire attached to a 9 V DC power supply. The four optical fibers coupled with Thorlabs photodetectors (DET 10A/M) at equal spacing of 25 mm on the block measured the combustion wave speed. The output of the photodetector was recorded with a Tektronix oscilloscope DPO 3054. The combustion wave speed was evaluated by time response voltage signal recorded in the oscilloscope obtained from the photodetector located at equal distance of 25 mm.

The pressurization rate of nanothermite composites was estimated by measuring the pressure generated during the combustion of 30 mg of CuO/Al nanothermite composite in a constant volume pressure cell of diameter of 6.25 mm and depth of 5 mm (Figure 1b). The nanothermite composits was loosely filled in the combustion chamber (with one end being blocked by a pressure sensor), maintaining a packing density of 0.2 g cm^{-3}, and was ignited via nichrome wire connected to a DC power source from the opposite end. A piezoelectric based pressure sensor PCB 119B12 having pressure measurement range of 0−827 MPa (PCB Piezotronics) was rigidly mounted over the combustion chamber to monitor the pressure signal. The charge output from the monitored pressure signal was applied to impedance converting amplifiers PCB 402A03 (PCB Piezotronics) in order to get low impedance voltage output. The signal output from PCB 402A03 was applied to a single-channel line operated signal conditioner PCB 482A21 (PCB Piezotronics) for constant current excitation and decoupling of the signal from DC bias voltage. The pressure signal from the signal conditioner PCB 482A21 was recorded by Tektronix digital oscilloscope, DPO3054.

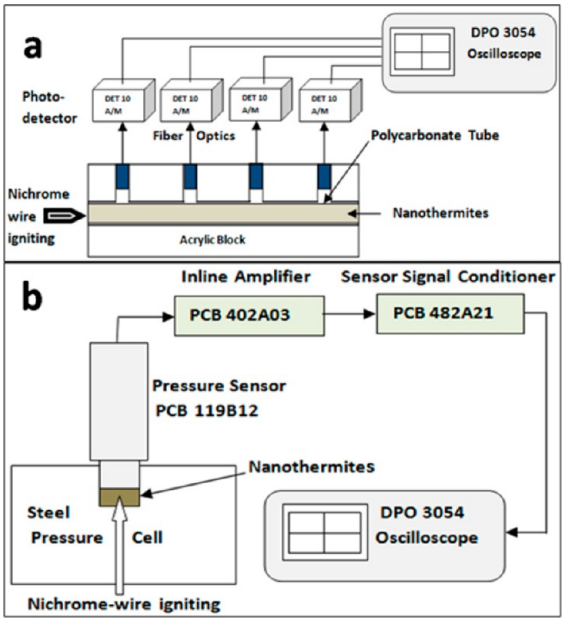

Figure 1. Schematic of experimental setup of (a) instrument burn tube for the measurement of combustion wave speed and (b) instrument pressure cell for the measurement of pressurization rate of nanothermites.

3. RESULTS AND DISCUSSION

We have biogenically synthesized short and long nanoscale size CuO nanorods (Figure 2) by replacing PEG400 in a solid-state reaction process[32] and PEG8000 in a sonoemulsion process[33] with Aloe vera gel, respectively. The X-ray diffraction patterns of CuO nanorods prepared by sonoemulsion biosynthesis and solid-state biosynthesis and their corresponding nanocomposites with assembled nanoaluminum (nAl) are represented in Figure 2a and b, respectively. All the XRD peaks of Figure 2a,b are consistent with JCPDS standard no. 48-1548 of CuO with a monoclinic phase. The absence of the peaks related to the $Cu(OH)_2$, Cu_2O, or precursor impurities indicates the formation of pure and single-phase CuO nanorods.

The morphology and structure of CuO nanorods developed by sonoemulsion and solid-state biosynthesis process were further characterized by transmission electron microscopy. The TEM images of CuO sample as developed by sonoemulsion biosynthesis process are shown in (Figure 2c, d, and Supporting Information Figure S1) which confirms the nanorods morphology with diameters of ca. 10−15 nm and lengths of up to 400 nm. The inset in Figure 2c represents the selected area diffraction (SAED) ring pattern of a bundle of CuO nanorods, showing highly polycrystalline structure of CuO nanorod bundles, while that of individual CuO nanorod, shown as Figure 2d (inset), reveals its single crystalline nature. Figure 2e represents the TEM image of CuO nanorods prepared by solid-state biosynthesis route with diameters of ca. 5−10 nm and lengths of up to 80 nm. The SAED ring pattern in this case shown as Figure 2e (inset) indicates polycrystalline monoclinic phase of the nanorods. Figure 2f represents the TEM image of CuO nanorods prepared by solid-state reaction using PEG400 surfactant. The yield of transformation of per unit gram of $CuCl_2 \cdot 2H_2O$ into CuO was measured to be approximately 0.49

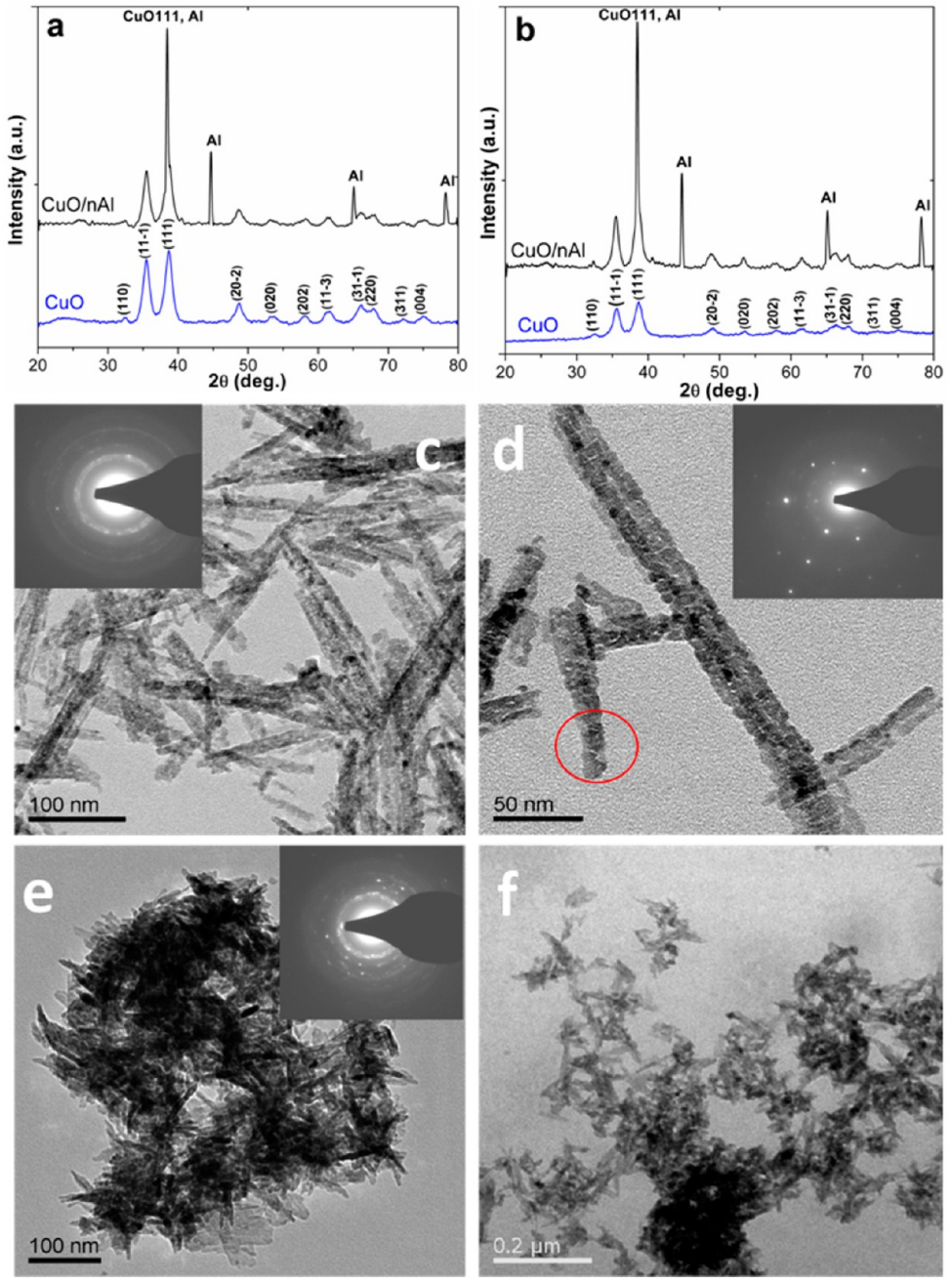

Figure 2. Powder X-ray diffraction pattern of (a) sonoemulsion biosynthesized CuO nanorods and nanothermite composites, (b) solid-state biosynthesized CuO nanorods and nanothermite composites. TEM images of (c, d) sonoemulsion biosynthesized CuO nanorods with inset of SAED pattern, (e) solid-state biosynthesized CuO nanorods with inset of SAED pattern, and (f) solid-state reaction synthesis of CuO nanorods.

g (as measured with a Citizen CX220 precision balance) for solid-state reaction synthesized CuO nanorods using PEG, and 0.55 g with sonoemulsion biosynthesized CuO nanorods.

3.1. Fourier Transform Infrared (FTIR) Analysis. Figure 3 represents the FTIR spectrum of CuO nanorods prepared by sonoemulsion and solid-state biogenic routes, and solid-state reaction synthesis using PEG400. The absorption peaks at 3416 cm^{-1} (CuO_{seb}) and 3418 cm^{-1} (CuO_{ssb}) could be attributed to the stretching vibration of adsorbed moisture and surface hydroxyl group related to the phenolic compounds.[3,53,54] The frequency bands at 1626 cm^{-1} of CuO_{seb} and 1624 cm^{-1} of CuO_{ssb} may be related to amide I bands associated with proteins[55] and/or vibrations due to −C═C functional groups from heterocyclic compounds.[56] The absorption peaks at 1495 cm^{-1} (CuO_{seb}) and 1480 cm^{-1} of CuO_{ssb} may be attributed to the stretching vibrations of carboxylate ion group of amino acid.[55] The phonon bands at 502 and 597 cm^{-1} (CuO_{ssb}), 495 and 586 cm^{-1} (CuO_{seb}), and 519 and 595 cm^{-1} (CuO_{peg}) correspond to the stretching vibration of Cu−O bond in monoclinic CuO.[57] The absorption peak at 1384 cm^{-1} in both spectra and 1050 cm^{-1} in CuO_{seb} could be appearing due to stretching vibrations of C−N functional groups of amines and −C−O−C− or −C−O− bonds of water-soluble heterocyclic compounds such as alkaloids and flavones.[57] The absorption peak appearing at 1591 and 3432 cm^{-1} of CuO_{peg} could be correlated to the bending and stretching vibrations of adsorbed water and surface hydroxyl groups.[58,59] The peak in the range of 600−1000 cm^{-1} (at 847 cm^{-1} with CuO_{peg}) is attributed to

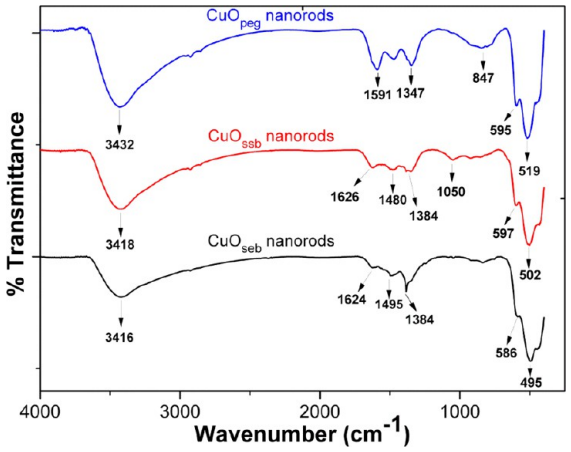

Figure 3. FTIR spectrum of CuO nanorods synthesized by sonoemulsion biosynthesis, solid-state biosynthesis, and solid-state reaction synthesis.

M−O stretching of CuO (M = Cu).[60] The absorption bands of 1300−1400 cm^{-1} (peak at 1347 cm^{-1} with CuO_{peg}) can be assigned to the adsorbed molecules of CO_2 and H_2O on CuO nanocrystals.[61]

3.2. Possible Reaction Mechanism. The solid-state and sonoemulsion biosynthesis routes in the presence of Aloe vera gel have been able to synthesize the self-assembled nanorods morphology of copper oxide which demonstrates the utility of Aloe vera gel as a biotemplate for anisotropic growth of copper oxide in both solid and emulsion phase reaction process. The FTIR measurement proves the presence of phenolic, carboxylic, and free amino groups adhered on the surface of CuO nanorods despite rigorous washing of the solutions. Proteins have been earlier suggested to bind with silver nanoparticles[55] and gold nanoparticles,[62] and also the presence of secondary layer capping of bioorganic compounds has been observed in Aloe-vera-synthesized CuO[16] and ZnO[17] nanoparticles. Accordingly, and from the FTIR measurements, the free amino and carboxylic groups could be considered to bind with the surface of nanoparticles and thus provide stability to the colloidal growth by preventing the agglomeration. The functional bonds such as −C═C, C−O−C, and C−O− derived from water-soluble compounds (alkaloids and flavones from the Aloe vera extract) may also be envisioned to provide capping action and participate or assist in the stabilization process of nanoparticles growth.[56] Overall, the amino, carboxylic, and phenolic functional groups of Aloe vera gel could be proposed to be responsible for the formation of copper oxide nanorods possessing the character very similar to the soft templates of poly(ethylene) glycol used in synthesis of CuO nanorods in solid-state reaction synthesis,[32] wet chemical synthesis,[63] and sonoemulsion synthesis.[33]

In solid-state biosynthesis, the formation of CuO nanorods was observed to occur instantly, forming black color slurry immediately upon mixing the reactants in presence of Aloe vera gel. The formation of CuO nanorods in solid-state biosynthesis was associated with heat and fume generation, indicating the reaction to be highly exothermic and also indicating the participation of Aloe vera gel. The higher concentration of hydroxyl ions derived from phenolic compounds of Aloe vera and the strong NaOH can be believed to transform the metastable $Cu(OH)_2$ instantly into CuO nanocrystals in support of generated heat. Increasing the aloe vera content from 3 to 5 mL in the solid-state biosynthesis process resulted in the formation of mixed nanostructures of nanorods and elongated nanoparticles (Figure 4a). It was observed that some nanorods were formed with size larger than 100 nm by increasing the Aloe vera content to 5 mL in the solid-state biosynthesis process. This improvement in size of nanorods may be attributed to increased growth kinetics of nanocrystals in a favorable medium of higher liquidity and increased hydroxyl ions released from the present phenolic compounds.

In sonoemulsion biosynthesis, $Cu(OH)_2$ is believed to gradually transform into CuO nanocrystals under the action of high frequency collisions of nucleated colloids in an ultrasonic bath set at a temperature of 60 °C. The long CuO nanorods formation in the emulsion phase could be attributed to the strongly oriented self-aggregation of the nanoparticles[64] guided by A. vera-sfg along energetically favored crystal planes. The TEM image in Figure 2d clearly manifests that the long CuO_{seb} nanorods are composed of many small nanoparticles oriently attached together.

An earlier report in this area has established the utility of the sonoemulsion[33] technique in the synthesis of long CuO nanorods, where it was suggested that the high frequency collisions of nanoparticles under dispersed conditions during ultrasonication increased the self-aggregation rate. The acoustic

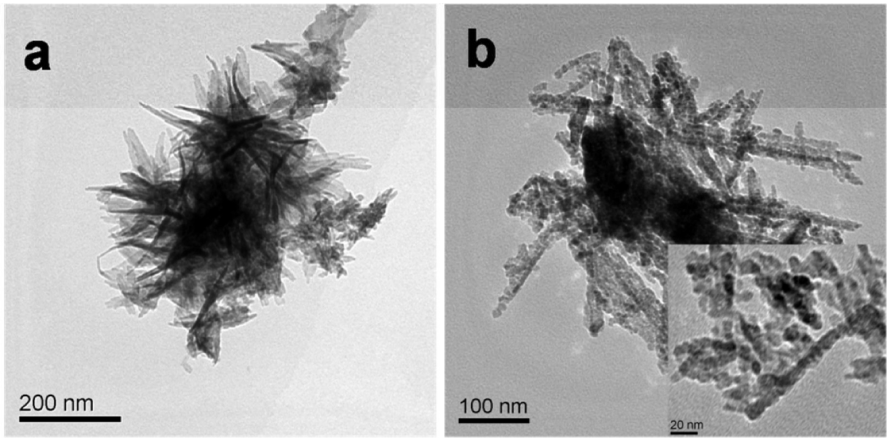

Figure 4. TEM image of CuO nanostructures using Aloe vera of (a) 5 mL in solid-state biosynthesis and (b) 2.5 mL in sonoemulsion biosynthesis process (inset is high-magnification TEM image).

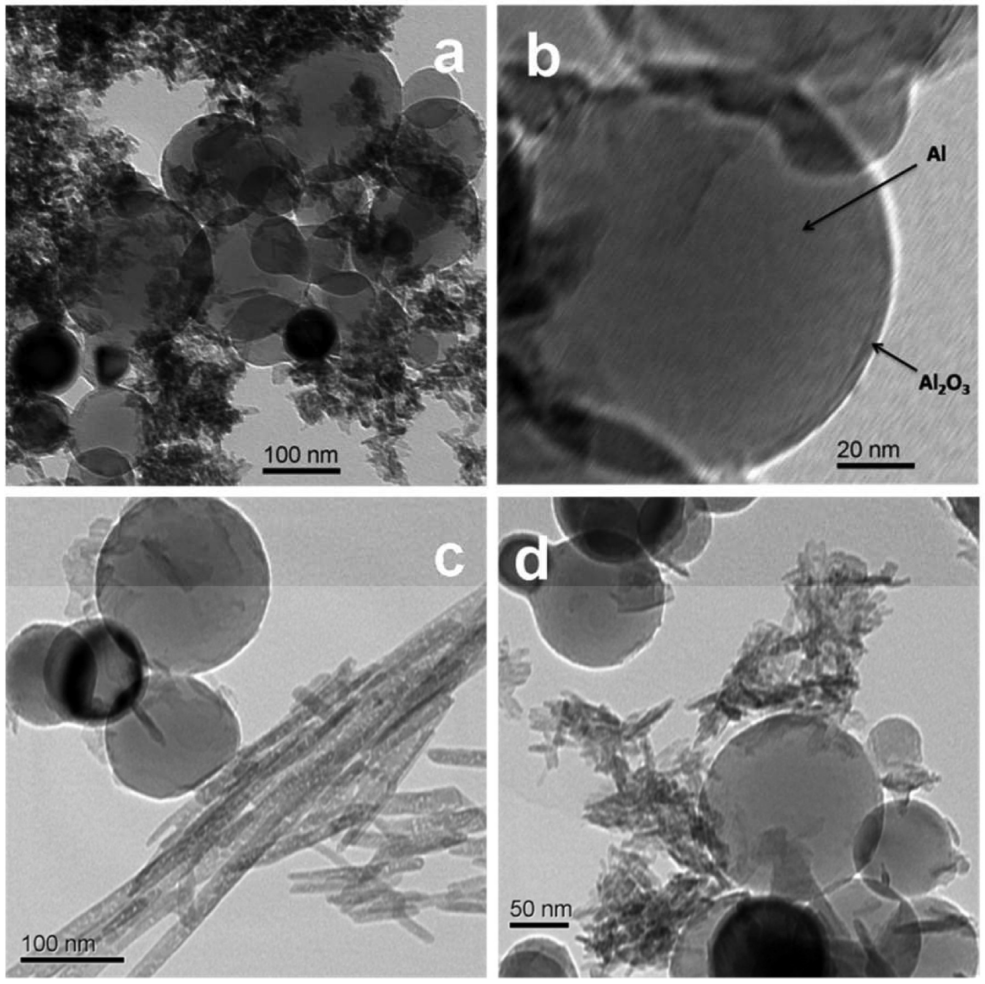

Figure 5. TEM images of nanothermite composites of (a, b) solid-state reaction synthesized CuO/nAl and CuO_{peg}/nAl. Panel (b) in specific shows the core−shell structure of the Al/Al_2O_3. (c) Sonoemulsion biosynthesized CuO/nAl, CuO_{seb}/nAl. (d) Solid-state biosynthesized CuO/nAl, CuO_{ssb}/nAl.

cavitations in the emulsion phase during ultrasonication are believed to produce shock waves, causing the nucleated particles to collide into one another and consequently producing internanoparticles fusion via melting at the contact surface.[65] Because the interparticle collision velocity depends on the size of particles,[65] the sufficiently aggregated nanoparticles experience less acceleration under cavitation shock waves than the newly born CuO colloids in the emulsion. Like PEG,[33,66,67] the adhered A. vera-sfg could be believed to provide steric hindrance effects confining the nanoparticle growth in certain direction. The level of steric hindrance effects on the shape and size evolution of CuO nanocrystals was studied by increasing the Aloe vera contents from 1.5 to 2.5 mL in sonoemulsion biosynthesis process, and it was observed that increasing the Aloe vera content mixed nanostructures of CuO nanoparticles and nanorods (shown in Figure 4b) were formed. From this observation, it can be illustrated that wherever the steric hindrance effects dominated against the self-aggregation rate, the nanoparticles were formulated. If they did not dominate, then the CuO nanorods were formulated. In the case of Aloe vera constituents of 1.5 mL, the level of steric hindrance is believed to be lower, and so the strong aggregation of nanoparticles causes the formation of long CuO nanorods. Therefore, the resulting driving force of the level of steric hindrance effects and varied self-aggregation rate of nanoparticles in the emulsion phase can be understood to govern the formation of various shape (nanoparticles/nanorods) and size distribution of CuO nanostructures.

The nucleation of $Cu(OH)_2$ and its transformation into CuO in emulsion-phase may be explained by considering the role of amino and carboxylate groups individually. Initially the Cu^{2+} is supposed to form $[Cu(NH_3)_4]^{+2}$ in the presence of amino groups ($-NH_2$), which upon addition of basic media of NaOH, converts first into $Cu(OH)_2$ then gets precipitated into $Cu(OH)_4^{2-}$ ions under excess of hydroxyl ions. The carboxylate functional group (COO−) may form copper oleate $[Cu(OA)_2]$[68,69] via interacting with Cu^{2+}. Because of weak affinity of $Cu(OA)_2$ with water,[69] $Cu(OH)_2$−OA is initially formed and then converted to $Cu(OH)_4^{2-}$ ions after interacting with excess hydroxyl ions. Cudennec and co-workers also proposed that the existence of hydroxyl ions enhanced the kinetics of transformation of divalent copper ions in to $Cu(OH)_4^{2-}$ in aqueous solution.[70] The hydroxyl ions derived from the phenolic functional groups may also partly enhance the formation of $Cu(OH)_4^{2-}$. The dynamics of formation of $Cu(OH)_4^{2-}$ and subsequently transformation in to CuO could be enhanced by the excess hydroxyl ions release from the added 2-propanol during the sonoemulsion biosynthesis process. Owing to the hydrophilicity and steric effect of hydroxyl ions, the $Cu(OH)_4^{2-}$ ions is thought to exist in spherical clusters,[71]

which transformed first to CuO_4 and then to CuO nanoparticles by losing two hydroxyl ions and one water molecule in a condensation phenomenon as reflected in the equation below.[70]

$$Cu^{2+} \xrightarrow{-NH_2/COO^-} [Cu(NH_3)_4{}^{2-}]/Cu(OA)_2$$
$$\rightarrow Cu(OH)_2$$
$$\rightarrow Cu(NH_3)_4{}^{2-}$$
$$\rightarrow CuO$$

3.3. Combustion Performance of CuO Nanorods/nAl Nanothermites. The combustion performance of nanothermite composites was evaluated by TG-DSC (thermogravimetric differential scanning calorimetry) measurement, combustion wave speed measurement, and pressure−time characteristics measurement of homogeneous mixture of nanoaluminum (nAl) with CuO nanorods biosynthesized as detailed above. Different equivalence ratios in the mixture were used for all characterization. The equivalence ratio was calculated by only considering the actual active aluminum content in core−shell of Al/Al_2O_3 nanoparticles. Figure 5a, c, d shows representative images of nanothermites of nAl with CuO nanorods synthesized by solid-state reaction process, sonoemulsion biosynthesis, and solid-state biosynthesis, respectively. From the high magnification TEM image of nanoaluminum shown in Figure 5b, the aluminum oxide layer was measured to be 4 nm. The equivalence ratio was formulated as

$$\text{equivalence ratio } (\Phi) = \frac{\left(\frac{\text{fuel}}{\text{oxidizer}}\right)_{\text{actual}}}{\left(\frac{\text{fuel}}{\text{oxidizer}}\right)_{\text{stoichiometry}}}$$

TG-DSC and combustion wave speed measurements were performed on nanothermites consisting of the oxidizers of long CuO nanorods synthesized by sonoemulsion biosynthesis (CuO_{seb}) and short CuO nanorods by solid-state biosynthesis (CuO_{ssb}), and solid-state reaction synthesis (CuO_{peg}) methods. The combustion wave speed of nanoaluminum with CuO nanorods developed by various synthesis routes is represented in Figure 6 and Supporting Information Table S1.

3.3.1. Combustion Wave Speed Measurement. The combustion process of biosynthesized CuO nanorods/nAl nanothermites has shown the specific characteristics of excess gas generation. From Figure 6, the combustion wave speed was found to be maximum at equivalence ratio of 1.6 (Supporting Information Figure S2) for all different synthesis routes of CuO nanorods used in the preparation of nanothermites. From Figure 6, it was also interpreted that the combustion performance of biosynthesized CuO nanorods/nAl nanothermites was relatively more stable than that of CuO_{peg}/nAl nanothermites in the excess-fuel combustion zone, that is, equivalence ratio of 1.6−1.8. Switching the equivalence ratio toward higher fuel contents from 1.6 to 1.8 was characterized by a lower variation in combustion wave speed (∼6% decrement with CuO_{seb}/nAl and ∼2.6% decrement with CuO_{ssb}/nAl) than the CuO_{peg}/nAl nanothermites showing 41% decrement in combustion wave speed. The main reason for this can be explained by hypothesizing that the surface functional groups burns completely in the presence of excess nanoaluminum and generates higher rate of gas release which greatly enhances the convection mode of heat transfer counteracting to some extent the negative effects of excess fuel rich combustion. Following the melt dispersion mechanism,[72] the melting of excess core active aluminum in high equivalence ratio nanothermites though increases the thermal conductivity of nanothermites but according to our views, the presence of unreacted fraction of nanoaluminum can also act as heat sink, which can be considered to decrease the combustion velocity. This is a generically observed phenomena in the case of nanostructured thermites, although as in the current biosynthesis there is presence of high-level hot gases in the combustion byproducts counteracting the heat sinking process. Thus, in the biosynthesized CuO-based nanothermites, the variation of the combustion wave speeds was a meager 6%.

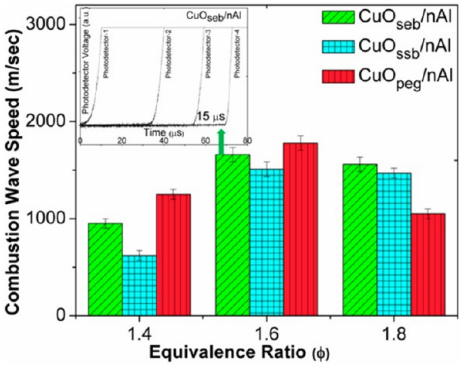

Figure 6. Combustion wave speed measurements of nanothermites as a function of equivalence ratio with inset of photodetector signal output vs time plot.

3.3.2. TG-DSC Measurement. Figure 7a represents the TG-DSC measurements of the nanothermites developed with nanoaluminum and solid-state reaction synthesized CuO nanorods (CuO_{peg}), solid-state biosynthesized CuO nanorods (CuO_{ssb}) and sonoemulsion biosynthesized CuO nanorods (CuO_{seb}). From TGA of nanothermites, the maximum weight loss observed up to 300 °C can be assigned to the weight-loss corresponding to the A. vera-sfg of CuO_{seb} and CuO_{ssb}, and adhered PEG-surface functional groups (PEG-sfg) with CuO_{peg}. The higher weight loss of 8.5% associated with CuO_{ssb}/nAl (9% with CuO_{peg}/nAl) nanothermites indicates that the A. vera-sfg (PEG-sfg in CuO_{peg}/nAl) adheres to a larger extent with the short CuO nanorods than the long CuO_{seb} nanorods (4.9% weight loss). This may be explained that in solid-phase biosynthesis some of the surface functional groups (free amino groups and/or alkaloids and flavones) and in solid-state reaction synthesis the PEG-sfg imposes a stronger steric hindrance like effects over nanoparticles growth and remained adhered to a larger extent with CuO nanoparticles than in sonoemulsion biosynthesis process. In the sonoemulsion biosynthesis process, the higher dynamics of nanoparticles growth caused by strong adhesion force within the nanoparticles overcomes the steric hindrance effects. The surface functional groups remain adherent in larger quantities with short CuO nanorods even after rigorous washing of CuO precipitates. The presence of higher quantity surface functional groups with short CuO_{ssb} nanorods modifies the combustion reaction more dominantly than the long CuO_{seb} nanorods based nanothermites.

In DSC studies, The CuO_{seb}/nAl nanothermites behave differently by undergoing a series of exothermic reactions observed at 509 °C (onset temperature of 501 °C, heat of reaction of 0.09 kJ g^{-1}), at 568 °C (onset temperature of 515

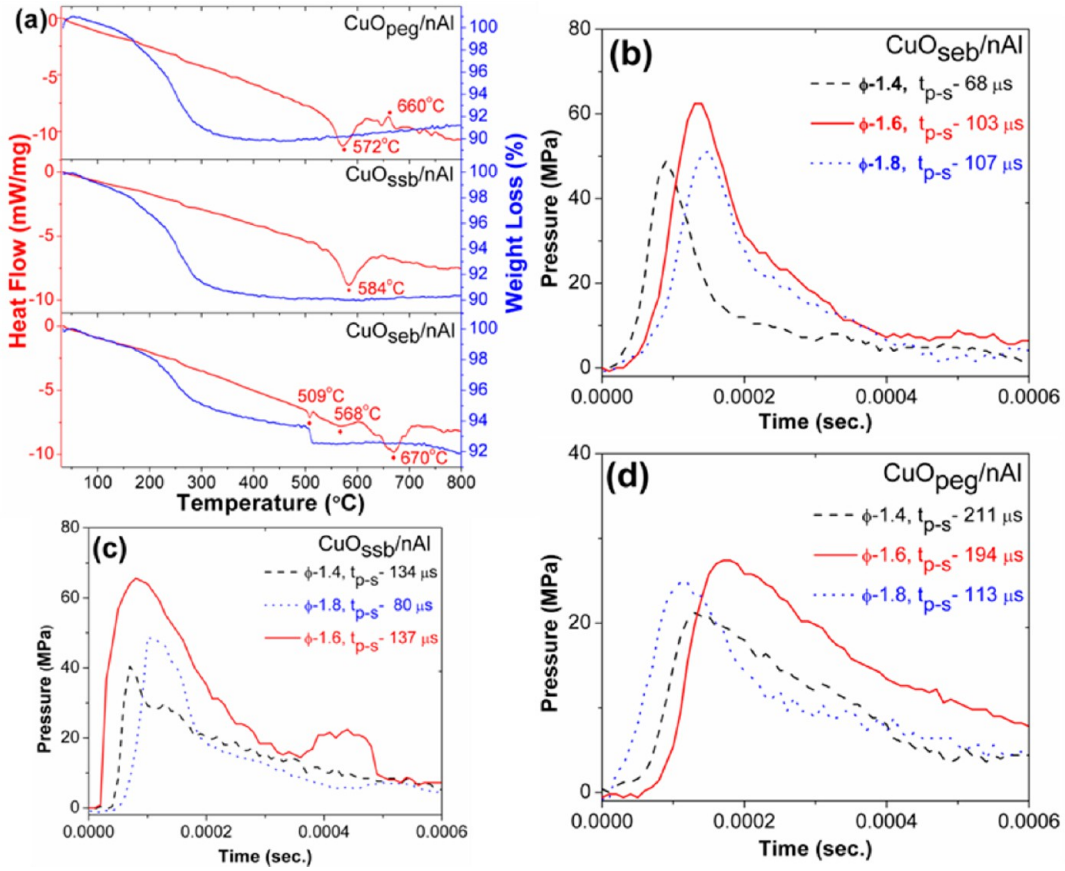

Figure 7. (a) TG-DSC measurements of CuO/nAl nanothermites at equivalence ratio of 1.6. (b–d) Dynamic pressure–time characteristics of CuO_{seb}/nAl, CuO_{ssb}/nAl, and CuO_{peg}/nAl nanothermites, respectively ($t_{p\text{-}s}$ is the pressure-sustain time at full width at half-maximum of normalized pressure–time curve).

°C, heat of reaction of 0.62 kJ g^{-1}), and at 670 °C (onset temperature of 604 °C, heat of reaction of 0.95 kJ g^{-1}). The low temperature exothermic peaks may occur due to low temperature redox reactions or interfacial Al–Cu–O recrystallization.[73] The exothermic peak for short nanorods based nanothermites (CuO_{ssb}/nAl) was observed at temperature of 584 °C (onset temperature of 516 °C) with a heat of reaction of 0.8 kJ g^{-1} which was much lower than the total heat of reaction of 1.66 kJ g^{-1} obtained with CuO_{seb}/nAl nanothermites. In DSC measurement of CuO_{peg}/nAl nanothermites, the exothermic peak was observed at 574 °C (onset temperature of 526 °C), producing the heat of reaction of 0.85 kJ g^{-1}. On the basis of nearly similar DSC characteristics data and adhered magnitude of surface functional groups of CuO_{ssb}/nAl and CuO_{peg}/nAl, it can be explained that it is the surface area in contact and purity of CuO nanorods which govern the exothermic reaction rather than the different nature of surface functional groups. This higher heat of reaction value obtained with CuO_{seb}/nAl nanothermites is very nearly comparable with that of the DNA-directed Al/CuO nanocomposites.[74] An intuitive explanation for higher heat of reaction value associated with CuO_{seb}/nAl nanothermites may be credited to the higher purity and surface area of the CuO_{seb} nanorods. It is believed that the possible thinner layer (owing to lower contents) of surface functional groups impairs the interatomic diffusion rate of CuO_{seb}/nAl nanothermites to a lesser extent than CuO_{ssb} based nanothermites. The low heat of reaction of CuO_{ssb}/nAl nanothermites decreases the temperature of exothermic reaction and so the rate of atomic diffusion responsible for low combustion wave speed in CuO_{ssb} based nanothermites than CuO_{seb} nanorods. Earlier work in this area has reported that during combustion a reduction in reaction temperature and diffusion rate decreases the reaction velocity.[75] The mechanism of exothermic reaction between biosynthesized CuO nanorods and nanoaluminum fuel may be explained by their relative characteristic length scale in nanothermite composites and the presence of A. vera-sfg affecting the intertransport distance between the fuel and oxidizer. The relative length scale of fuel and oxidizer decides not only the intertransport distance but also the relative strength of fuel or oxidizer in nanothermite composites acting as either fuel or oxidizer rich nanothermites. For the same average size of nanoaluminum, that is, 80 nm and equivalence ratio, the short CuO nanorods participate in exothermic reaction with higher shared surface area with nanoaluminum, and so higher available oxygen atoms apparently make the nanothermites slightly oxidizer rich. This may be the reason that, at equivalence ratio of 1.8, the oxidizer rich nature of the short CuO_{ssb} nanorods based nanothermites (CuO_{ssb}/nAl) react with higher nanoaluminum contents than at equivalence ratio of 1.6, and therefore, a lower fraction of unreacted nanoaluminum imposes lesser heat sink effect and so a lower variation in combustion wave speed was observed from switching equivalence ratio from 1.6 to 1.8.

3.3.3. Pressure–Time Characteristics Measurement. The measured value of maximum pressure, pressurization, rate and pressure-sustain time ($t_{p\text{-}s}$) of nanothermites at various equivalence ratios are shown Figure 7b–d and Supporting

Information Figure S3, Table S1. Here, the pressure-sustain time ($t_{p\text{-}s}$) is defined by the time duration at which the pressure magnitude corresponding to full width at half-maximum (fwhm) of normalized pressure−time characteristics curve, sustained. The pressure−time characteristics curve of CuO_{seb}/nAl (Figure 7b) was observed to be more uniform and smoother than the CuO_{ssb}/nAl nanothermites (Figure 7c). Because the surface functional groups are believed to be more uniformly distributed in emulsion phase than in solid-state phase, they adhere more uniformly and also in lesser quantity with CuO_{seb} nanorods than CuO_{ssb}, and therefore, the combustion process in CuO_{seb}/nAl nanothermites is attributed to propagation in a uniform and smoother way. Despite the low percentage of Aloe vera surface functional groups in CuO_{seb}, the pressure magnitude of its nanothermites was very similar to that of CuO_{ssb} based nanothermites at all equivalence ratios; therefore, it can be concluded that the high heat of reaction value associated with high aspect CuO_{seb} contributes to a major proportion of pressure buildup due to high rate of atomic diffusion during the exothermic reaction. When the pressure-sustain time was compared for various nanothermites, the lowest pressure-sustain time was observed with CuO_{seb}/nAl, which also confirms our previous conclusion that the pressure buildup is more dominated by atomic diffusion process than gas generated by surface functional groups owing to high aspect CuO_{seb} nanorods. The presence of higher quantity A. vera-sfg in CuO_{ssb}/nAl nanothermites (Figure 7c) causes the increase in pressure-sustain time very similar to the case the loading of acrylamidomethyl cellulose acetate butyrate polymer in Fe_2O_3/Al nanothermite composites.[76] The maximum peak pressure and pressurization rate for each synthesis route of CuO nanorods were observed at equivalence ratio of 1.6 (see the comparison in Figure 8). From Figure 8, the biosynthesized

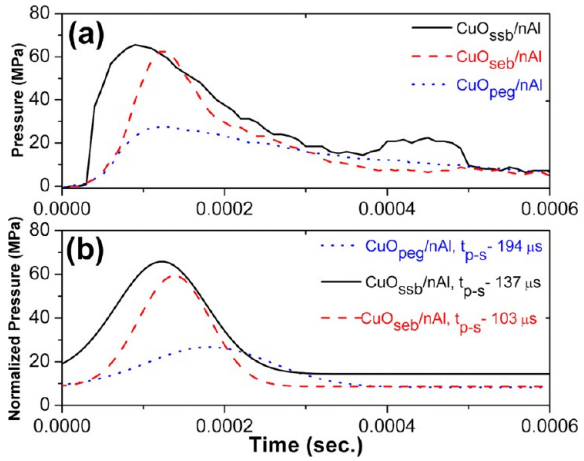

Figure 8. (a) Dynamic pressure−time characteristics. (b) Normalized dynamic pressure−time characteristics of CuO/nAl nanothermites at equivalence ratio of 1.6.

CuO nanorods evidently developed a very high pressure magnitude of 62.4 ± 4 MPa (pressurization rate of 0.62 ± 0.2 MPa/μs) with CuO_{seb}/nAl and 65.6 ± 4 MPa (~2.4 times of CuO_{peg}/nAl nanothermites) with CuO_{ssb}/nAl and, pressurization rate of 1.09 ± 0.2 MPa/μs (this is more than 4 times that of CuO_{peg}/nAl) with CuO_{ssb}/nAl. The higher maximum pressure and pressurization rate associated with biosynthesized CuO nanorods oxidizers based nanothermites could be attributed to its higher rate of gas generation by burning of A. vera-sfg during the combustion than CuO_{peg}/nAl nanothermites. The highest pressurization rate developed by CuO_{ssb} oxidizers could be attributed to its highest gas generating abilities due to burning of higher quantity adhered surface functional groups in the same time domain of combustion CuO_{seb} and CuO_{peg} based nanothermites.

4. CONCLUSIONS

In conclusion, this paper reports Aloe vera gel as biotemplating/capping agent for green synthesis of CuO nanorods in both solid and emulsion phase reaction process which also served as catalyst enhancing the reactivity of CuO oxidizers via excess gas release during the exothermic reaction with nanoaluminum. The typical gas generating role of Aloe vera that adheres as surface functional groups on CuO nanostructures leads to marked improvements in the combustion and pressure generation properties of the composites. Both Aloe vera assisted processes, that is, solid-state biosynthesis and sonoemulsion biosynthesis, are realized to develop uniform CuO nanorods of different characteristic lengths where the sonoemulsion biosynthesis process has been found to produce longer CuO nanorods with diameters of ca. 10−15 nm and lengths of up to 400 nm. The biosynthesized CuO oxidizers are able to create high-energy nanothermite composites developing a high heat of reaction value of 1.66 kJ g^{-1}. The biosynthesized CuO nanorods have the outstanding ability of abundant gas generation which delivered 2.3 times higher pressure magnitude and 4 times higher pressurization rate of PEG400 assisted CuO nanorods/nAl nanothermites. The quantity of surface functional groups from Aloe vera has been found to be responsible for governing the dynamic pressure characteristics of nanothermites.

■ ASSOCIATED CONTENT

Supporting Information

TEM image of sonoemulsion biosynthesized CuO nanorods showing varied-size distribution. Table of combustion wave speed and pressure−time measurements of various nanothermites, comparison of combustion wave speed (photodetector signal output vs time plot) of nanothermites developed with the oxidizer of CuO nanorods synthesized by various methods at equivalence ratio of 1.6, and normalized pressure-time characteristics curve of various nanothermites. This material is available free of charge via the Internet at http://pubs.acs.org.

■ AUTHOR INFORMATION

Corresponding Author

*E-mail: bhattacs@iitk.ac.in.

Notes

The authors declare no competing financial interest.

■ ACKNOWLEDGMENTS

We express our sincere thanks to Science Engineering and Research Council, Department of Science and Technology (DST), Government of India for its financial support. The author would also like to acknowledge Department of Materials Science and Engineering and Nanoscience Centre of IIT Kanpur for providing good material characterization facilities. V.K.P. sincerely acknowledges All India Council for Technical Education, Government of India and G B Pant Engineering College, Pauri-Garhwal (Uttarakhand) for sponsoring and

supporting him to pursue Ph.D. studies at IIT Kanpur under Quality Improvement Programme (QIP). The authors also thank Netzsch Technologies India Pvt Ltd Chennai for its TG-DSC analysis.

REFERENCES

(1) Akhtar, M. S.; Panwar, J.; Yun, Y. S. *ACS Sustainable Chem. Eng.* **2013**, *1*, 591−602.
(2) Kharissova, O. V.; Dias, H. V.; Kharisov, B. I.; Pérez, B. O.; Pérez, V. M. J. *Trends Biotechnol.* **2013**, *31*, 240−248.
(3) Chandran, S. P.; Chaudhary, M.; Pasricha, R.; Ahmad, A.; Sastry, M. *Biotechnol. Prog.* **2006**, *22*, 577−583.
(4) Shankar, S. S.; Rai, A.; Ahmad, A.; Sastry, M. *Chem. Mater.* **2005**, *17*, 566−572.
(5) Shankar, S. S.; Rai, A.; Ankamwar, B.; Singh, A.; Ahmad, A.; Sastry, M. *Nat. Mater.* **2004**, *3*, 482−488.
(6) Shankar, S. S.; Ahmad, A.; Pasricha, R.; Sastry, M. *J. Mater. Chem.* **2003**, *13*, 1822−1826.
(7) Philip, D.; Unni, C. *Phys. E (Amsterdam, Neth.)* **2011**, *43*, 1318−1322.
(8) Kotakadi, V. S.; Rao, Y. S.; Gaddam, S. A.; Prasad, T. N. V. K. V.; Reddy, A. V.; Gopal, D. V. R. *Colloids Surf., B* **2013**, *105*, 194−198.
(9) Bindhu, M. R.; Umadevi, M. *Spectrochim. Acta, Part A* **2013**, *101*, 184−190.
(10) Ghodake, G. S.; Deshpande, N. G.; Lee, Y. P.; Jin, E. S. *Colloids Surf., B* **2010**, *75*, 584−589.
(11) Danthal, P.; Mukhopodhyay, M. *Ind. Eng. Chem. Res.* **2012**, *51*, 13014−13020.
(12) Umadevi, M.; Bindhu, M. R.; Sathe, V. *J. Mater. Sci. Technol.* **2013**, *29*, 317−322.
(13) Sathishkumar, M.; Sneha, K.; Won, S. W.; Cho, C. W.; Kim, S.; Yun, Y. S. *Colloids Surf., B* **2009**, *73*, 332−338.
(14) Raghunandan, D.; Bedre, M. D.; Basavaraja, S.; Sawle, B.; Manjunath, S. Y.; Venkataraman, A. *Colloids Surf., B* **2010**, *79*, 235−240.
(15) Duran, N.; Seabra, A. B. *Appl. Microbiol. Biotechnol.* **2012**, *95*, 275−288.
(16) Gunalan, S.; Sivaraj, R.; Venckatesh, R. *Spectrochim. Acta, Part A* **2012**, *97*, 1140−1144.
(17) Sangeetha, G.; Rajeshwari, S.; Venckatesh, R. *Mater. Res. Bull.* **2011**, *46*, 2560−2566.
(18) Samat, N. A.; Nor, R. M. *Ceram. Int.* **2012**, *39*, 545−548.
(19) Maensiri, S.; Laokul, P.; Klinkaewnarong, J.; Phokha, S.; Promarak, V.; Seraphin, S. *J. Optoelectron. Adv. Mater.* **2008**, *10*, 161−165.
(20) Herrera-Becerra, R.; Zorrilla, C.; Ascencio, J. A. *J. Phys. Chem. C* **2007**, *111*, 16147−16153.
(21) Herrera-Becerra, R.; Rius, J. L.; Zorrilla, C. *Appl. Phys. A: Mater. Sci. Process.* **2010**, *100*, 453−459.
(22) Phumying, S.; Labuayai, S.; Thomas, C.; Amornkitbamrung, V.; Swatsitang, E.; Maensiri, S. *Appl. Phys. A: Mater. Sci. Process.* **2013**, *111*, 1187−1193.
(23) Gandhi, R. R.; Gowri, S.; Suresh, J.; Selvam, S.; Sundrarajan, M. *J. Biobased Mater. Bioenergy* **2012**, *6*, 204−208.
(24) Reitz, J. B.; Solomon, E. I. *J. Am. Chem. Soc.* **1998**, *120*, 11467−11478.
(25) Frietsch, M.; Zudock, F.; Goschnick, J.; Bruns, M. *Sens. Actuators, B* **2000**, *65*, 379−381.
(26) Gao, X. P.; Bao, J. L.; Pan, G. L.; Zhu, H. Y.; Huang, P. X.; Wu, F.; Song, D. Y. *J. Phys. Chem. B* **2004**, *108*, 5547−5551.
(27) Maruyama, T. *Sol. Energy Mater. Sol. Cells* **1998**, *56*, 85−92.
(28) Shende, R.; Subramanian, S.; Hasan, S.; Apperson, S.; Thiruvengadathan, R.; Gangopadhyay, K.; Gangopadhyay, S.; Redner, P.; Kapoor, D.; Nicolich, S.; Balas, W. *Propellants, Explos., Pyrotech.* **2008**, *33*, 122.
(29) Jian, G. Q.; L. Liu, L.; Zachariah, M. R. *Adv. Funct. Mater.* **2013**, *23*, 1341−1346.
(30) Adánez, J.; Gayán, P.; Celaya, J.; de.Diego, L. F.; García-Lubiano, F.; Abad, A. *Ind. Eng. Chem. Res.* **2006**, *45*, 6075−6080.
(31) Cao, Y.; Casenas, B.; Pan, W. P. *Energy Fuels* **2006**, *20*, 1845−1854.
(32) Wang, W.; Zhan, Y.; Wang, X.; Liu, Y.; Zheng, C.; Wang, G. *Mater. Res. Bull.* **2002**, *37*, 1093−1100.
(33) Patel, V. K. *J. Cluster Sci.* **2013**, *24*, 821−828.
(34) Zhu, L.; Chen, Y.; Zheng, Y.; Li, N.; Zhao, J.; Sun, Y. *Mater. Lett.* **2010**, *64*, 976−979.
(35) Poizot, P.; Hung, C. J.; Nikiforov, M. P.; Bohannan, E. W.; Switzer, J. A. *Electrochem. Solid-State Lett.* **2003**, *6*, 21−25.
(36) Jiang, X.; Herricks, T.; Xia, Y. *Nano Lett.* **2002**, *2*, 1333−1338.
(37) Reynolds, T.; Dweck, A. C. *J. Ethnopharmacol.* **1999**, *68*, 3−37.
(38) Rodríguez-Rodríguez, E.; Martín, D.; Díaz-Romero, C. *Crit. Rev. Food Sci. Nutr.* **2010**, *50*, 305−326.
(39) Shin, K. H.; Woo, W. S.; Lim, S. S.; Shim, C. S.; Chung, H. S.; Kennely, E. J.; Kinghorn, A. D. *J. Nat. Prod.* **1997**, *60*, 1180−1182.
(40) Umano, K.; Nakahara, K.; Shoji, A.; Shibamoto, T. *J. Agric. Food Chem.* **1999**, *47*, 3702−3705.
(41) Saccu, D.; Bagoni, P.; Procida, G. J. *J. Agric. Food Chem.* **2001**, *49*, 4526−4530.
(42) Aumann, C. E.; Skofronick, G. L.; Martin, J. A. *J. Vac. Sci. Technol., B: Microelectron. Nanometer Struct.—Process., Meas., Phenom.* **1995**, *13*, 1178−1183.
(43) Fischer, S. H.; Grubelich, M. C. Theoretical energy release of thermites, intermetallics, and combustible metals. *Proceedings of 24th International Pyrotechnics Seminar*, Monterey, CA, 1998; pp 231−286 (also a Sandia Technical Report, No. SAND98-1176C).
(44) Rossi, C.; Zhang, K.; Esteve, D.; Alphonse, P.; Tailhades, P.; Vahlas, C. *J. Microelectromech. Syst.* **2007**, *16*, 919−931.
(45) Dreizin, E. L. *Prog. Energy Combust. Sci.* **2009**, *35*, 141−167.
(46) Son, S. F.; Asay, B. W.; Foley, T. J.; Yetter, R. A.; Wu, M. H.; Risha, G. A. *J. Propul. Power* **2007**, *23*, 715−721.
(47) Apperson, S. J.; Bezmelnitsyn, A. V.; Thiruvengadathan, R.; Gangopadhyay, K.; Gangopadhyay, S.; Balas, W. A.; Anderson, P.; Nicolich, S. *J. Propul. Power* **2009**, *25*, 1086−1091.
(48) Pezous, H.; Rossi, C.; Sanchez, M.; Mathieu, F.; Dollat, X.; Charlot, S.; Salvagnac, L.; Conédéra, V. *Sens. Actuators, A* **2010**, *159*, 157−167.
(49) Korampally, M.; Apperson, S. J.; Staley, C. S.; Castorena, J. A.; Thiruvengadathan, R.; Gangopadhyay, K.; Mohan, R. R.; Ghosh, A.; Polo-Parada, L.; Gangopadhyay, S. *Sens. Actuators, B* **2012**, *171−172*, 1292−1296.
(50) Apperson, S.; Shende, R. V.; Subramanian, S.; Tappmeyer, D.; Gangopadhyay, S.; Chen, Z.; Gangopadhyay, K.; Redner, P.; Nicholich, S.; Kapoor, D. *Appl. Phys. Lett.* **2007**, *91*, 243109−243109−3.
(51) Thiruvengadathan, R.; Bezmelnitsyn, A.; Apperson, S.; Staley, C.; Redner, P.; Balas, W.; Nicolich, S.; Kapoor, D.; Gangopadhyaya, K. *Combust. Flame* **2011**, *158*, 964−978.
(52) Plantier, K. B.; Pantoya, M. L.; Gash, A. E. *Combust. Flame* **2005**, *140*, 299−309.
(53) Karuppuchamy, S.; Jeong, J. M. *J. Oleo Sci.* **2006**, *55*, 263−266.
(54) Xu, Y.; Chen, D.; Jiao, X.; Xue, K. *Mater. Res. Bull.* **2007**, *42*, 1723−1731.
(55) Shankar, S. S.; Ahmad, A.; Sastry, M. *Biotechnol. Prog.* **2003**, *19*, 1627−1631.
(56) Huang, J.; Li, Q.; Sun, D.; Lu, Y.; Su, Y.; Yang, X.; Wang, H.; Wang, Y.; Shao, W.; He, N.; Hong, J.; Chen, C. *Nanotechnology* **2007**, *18*, 105104.
(57) Nyquist, R. A.; Kagel, R. O. *Infrared Spectra of Inorganic Compounds*; Academic Press: New York, 1971; 220.
(58) Xu, Y.; Chen, D.; Jiao, X.; Xue, K. *Mater. Res. Bull.* **2007**, *42*, 1723−1731.
(59) Gao, X. P.; Bao, J. L.; Pan, G. L.; Zhu, H. Y.; Huang, P. X.; Wu, F.; Song, D. Y. *J. Phys. Chem. B* **2004**, *108*, 5547−5551.
(60) Abdelaziz, M.; Abdelrazek, E. M. *Phys. B* **2007**, *390*, 1−7.
(61) Chen, C.; Zheng, Y.; Zhan, Y.; Lin, X.; Zheng, Q.; Wei, K. *Cryst. Growth Des.* **2008**, *8*, 3549−3554.

(62) Gole, A.; Dash, C. V.; Ramachandran, V.; Mandale, A. B.; Sainkar, S. R.; Rao, M.; Sastry, M. *Langmuir* **2001**, *17*, 1674−1679.
(63) Wang, W.; Liu, Z.; Liu, Y.; Xu, C.; Zheng, C.; Wang, G. *Appl. Phys. A: Mater. Sci. Process.* **2003**, *76*, 417−420.
(64) Leite, E. R.; Lee, E. J. H.; Ribeiro, C.; Longo, E. *J. Phys. Chem. B* **2005**, *109*, 20842−20846.
(65) Doktycz, S. J.; Suslick, K. S. *Science* **1990**, *247*, 1067−1069.
(66) Li, Z.; Xiong, Y.; Xie, Y. *Inorg. Chem.* **2003**, *42*, 8105−8109.
(67) Zhang, D. S.; Fu, H. X.; Shi, L. Y.; Pan, C. S.; Li, Q.; Chu, Y. L.; Yu, W. J. *Inorg. Chem.* **2007**, *46*, 2446−2451.
(68) Bao, N. Z.; Shen, L. M.; An, W.; Padhan, P.; Turner, H.; Gupta, A. *Chem. Mater.* **2009**, *21*, 3458−3468.
(69) Zhao, Y.; Zhao, J. Z.; Li, Y. L.; Ma, D. C.; Hou, S. N.; Li, L. Z.; Hao, X. L.; Wang, Z. C. *Nanotechnology* **2011**, *22*, 115604.
(70) Cudennec, Y.; Lecerf, A. *Solid State Sci.* **2003**, *5*, 1471−1474.
(71) Cölfen, H.; Mann, S. *Angew. Chem., Int. Ed.* **2003**, *42*, 2350−2365.
(72) Levitas, V. I.; Asay, B. W.; Son, S. F.; Pantoya, M. L. *Appl. Phys. Lett.* **2006**, *89*, 071909.
(73) Kwon, J.; Ducéré, J. M.; Alphonse, P.; Bahrami, M.; Petrantoni, M.; Veyan, J.-F.; Tenailleau, C.; Estève, A.; Rossi, C.; Chabal, Y. J. *ACS Appl. Mater. Interfaces* **2013**, *5*, 605−613.
(74) Severac, F.; Alphonse, P.; Esteve, A.; Bancaud, A.; Rossi, C. *Adv. Funct. Mater.* **2012**, *22*, 323−329.
(75) Gavens, A. J.; Van Heerden, D.; Mann, A. B.; Reiss, M. E.; Weihs, T. P. *J. Appl. Phys.* **2000**, *87*, 1255−1263.
(76) Bezmelnitsyn, A.; Thiruvengadathan, R.; Barizuddin, S.; Tappmeyer, D.; Apperson, S.; Gangopadhyay, K.; Gangopadhyay, S.; Redner, P.; Donadio, M.; Kapoor, D.; Nicolich, S. *Propellants, Explos., Pyrotech.* **2010**, *35*, 384−394.